# Distortion in p-i-n Diode Control Circuits

ROBERT H. CAVERLY, MEMBER, IEEE, AND GERALD HILLER, MEMBER, IEEE

*Abstract*—**Traditionally, distortion in p-i-n diodes has been thought to be only a function of the carrier lifetime and frequency of operation. This understanding is based on empirical evidence and is not entirely accurate. This paper will discuss the origins of p-i-n diode distortion and study the effects of various devices parameters on distortion performance. Included in the investigation on single-diode circuits will be switching circuits and reflective attenuators. In switch circuits, the analysis shows that distortion can be minimized by maximizing the stored-to-charge resistance ratio in the diode. In attenuators, the analysis shows that maximizing the i-region thickness will minimize distortion, independent of the device carrier lifetime. In attenuators where multiple p-i-n diodes are used (the bridged-tee and PI are discussed), maximizing the i-region thickness also minimizes the distortion, independent of carrier lifetime. The model accurately predicts distortion signal cancellation in both single and multiple p-i-n diode circuits.**

## NOMENCLATURE

| | |
|---|---|
| $A$ | cross-sectional area of p-i-n diode. |
| $D$ | Ambipolar diffusion constant $= \mu V_T$. |
| $f_k$ | Frequency. |
| $I_k$ | Applied RF current. |
| $I_H$ | Harmonic currents. |
| $I_{IM}$ | Intermodulation currents. |
| IP | Distortion intercept points. |
| $I_i(t)$ | Total diode current. |
| $I_0$ | DC bias current. |
| $i(t)$ | RF drive current. |
| $k$ | Boltzmann's constant. |
| $j$ | $\sqrt{-1}$. |
| $L$ | Diffusion length $= \sqrt{D\tau}$. |
| $L_k$ | RF diffusion length $= L/\sqrt{1+j\omega_k\tau}$. |
| $L_{2a}$ | Second harmonic power. |
| $L_{3a}$ | Third harmonic power. |
| $L_{ab}$ | Second-order intermodulation power. |
| $L_{2ab}$ | Third-order intermodulation power. |
| $n_k$ | RF injected charge density. |
| $n_0$ | DC injected charge density. |
| $q$ | Electron charge. |
| $Q$ | Stored dc charge $= I_0\tau$. |
| $\mu_n$ | Electron mobility. |
| $\mu_p$ | Hole mobility. |
| $\mu$ | Ambipolar mobility $= 2\mu_n\mu_p/(\mu_n+\mu_p)$. |
| $R_s$ | i-region series resistance. |
| $T$ | Temperature (300 K). |
| $\tau$ | Carrier lifetime. |
| $V_\tau$ | $kT/q$. |
| $\omega_k$ | $2\pi f_k$. |
| $W$ | i-region thickness. |
| $x$ | Depth into i-region from boundary. |

Manuscript received July 31, 1986; revised December 22, 1986.

R. H. Caverly is with the Department of Electrical and Computer Engineering, Southeastern Massachusetts University, N. Dartmouth, MA 02747.

G. Hiller is with M/A-COM Semiconductor Products, Burlington, MA 01803.

IEEE Log Number 8613464.

## I. INTRODUCTION

USE is commonly made of p-i-n diodes to control the amplitude of radio frequency (RF) and microwave signals in attenuator and switch circuits. An ideal p-i-n diode will perform this function without distorting the applied signal. However, the p-i-n diode has a specific nonlinear high-frequency current–voltage characteristic; thus, there will be harmonically related signals generated by the p-i-n diode. This paper is concerned with the distortion generated by p-i-n diode switches and attenuators. The nonlinear mechanisms are analyzed, and equations are developed that allow designers to predict second- and third-order harmonic and intermodulation products in a forward-biased p-i-n diode. The analytic expressions are verified by experimental data.

The interest in p-i-n diode distortion has become more significant as these devices are used at frequencies in the VHF, UHF, and RF bands. As p-i-n diodes are employed in lower frequency applications, particularly in sensitive receivers where multiple signals are simultaneously received, the generation of in-band intermodulation signals can seriously affect receiver sensitivity.

Even at microwave frequencies, the distortion generated in the form of harmonics is often an important system performance criterion. This may be particularly significant in high-power phase shifter and switch applications.

Traditionally, distortion in p-i-n diodes has been related to the frequency and the minority carrier lifetime. A figure of merit, based upon the assumption that the RF signal removes all stored charge if its period is equivalent to the minority carrier lifetime, has been an empirically accepted measure of the lower frequency limit of p-i-n diodes. This measure is partially true and was experimentally supported when experiments replaced fast-carrier-lifetime p-i-n diodes with slower ones with reported improvement in distortion. The experimenter may not have realized that the better device had a different geometry and that this also contributed to its lower distortion.

The effect of conductivity modulation on p-i-n diodes was recognized by Leenov in his classic paper on the RF properties of p-i-n diodes [1]. Leenov calculated the RF and dc injected charge densities as functions of depth into the i-region, shown in Fig. 1, and indicated that the RF injected charges are concentrated only near the i-region

0018-9480/87/0500-0492$01.00 ©1987 IEEE

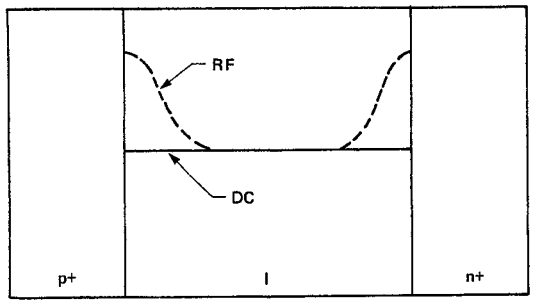


Fig. 1. Graph of ac and dc i-region charge densities injected from the heavily doped end regions of the p-i-n diode. --- RF. —— dc.

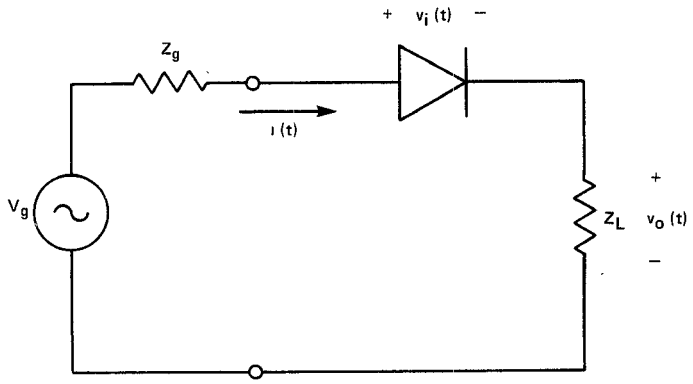


Fig. 2. The high-frequency p-i-n diode circuit (bias structure not shown).

boundaries, whereas the dc injected charges are relatively constant throughout the i-region. The modulation of the i-region conductance by carrier injection from the applied ac signal produces harmonic and intermodulation distortion currents at the diode output. Measurements of distortion in shunt attenuators at 40 and 60 MHz have been performed by Lepoff [2], and his results show local minima at certain attenuation levels as well as a dependence of the distortion level on bias current. Caulton *et al.* [3] have made distortion measurements on high-power p-i-n diode circuits at frequencies as low as 500 kHz, and they discuss, independently, the effects of lifetime and i-region thickness on distortion performance. Other investigators have also reported experimental observations of p-i-n diode distortion in switching circuits [4], [5], and Hiller and Caverly [6] have quantified the distortion intercept points in single-diode switching circuits as functions of the dc stored-charge-to-resistance ratio.

Mathematical models have been advanced by several investigators to describe the generated output spectra of the p-i-n diode using both Taylor and Volterra series representations in their analyses [6]–[9]. The Volterra series models of Albrecht and Jensen [7] and Reiss [9] show good agreement with the limited experimental data on single- and multidiode attenuators presented in their papers. One particular model, that advanced by Reiss [8], provides a means of mathematically describing the device nonlinearities in terms of a Taylor series expansion as well as device parameters that are readily measured. Absent in any of the works cited, however, have been an in-depth study of those diode and circuit parameters that control the level of distortion in single and multiple p-i-n diode control circuits, and any experimental verification of analytic expressions.

## II. Analysis

### A. Nonlinear Model of the Forward-Biased p-i-n Diode

A nonlinear model applicable to RF and microwave frequencies is necessary to determine the distortion characteristics of the p-i-n diode. The basic circuit used for the model, shown in Fig. 2, shows a series-connected diode between a generator ($V_g, Z_g$) and a load $Z_l$ (the diode biasing network is not shown). Here, $Z_g = Z_l = Z_0$, where $Z_0$ is the characteristic impedance of the transmission lines connecting various circuit components. At high frequencies, the entire RF voltage appears primarily across the i-region [8], [10], so that only the i-region nonlinear voltage–current relationship needs to be determined. A nonlinear model that describes the voltage developed across a p-i-n diode as a function of multiple RF driving currents through the device has been developed by Reiss [8]; it was derived under the following assumptions: 1) one-dimensional i-region charge density variations; 2) high dc injection of carriers from the heavily doped end regions; 3) Shockley–Hall–Read recombination; and 4) quasi neutrality of the injected carriers in the i-region.

The i-region ac voltage drop as a result of a distortion-free RF drive current of the form

$$i(t) = \sum_{k=1}^{K} I_k \cos(\omega_k t)$$

can be written as [8]

$$v_i(t) = \frac{i(t)}{Aq\mu} \cdot \int_0^{W/2} dx \left\{ n_0(x) \left[ 1 + \mathrm{RE} \left\{ \sum_{k=1}^{K} \frac{n_k(x)}{n_0(x)} e^{j\omega_k t} \right\} \right] \right\}^{-1} \quad (1)$$

where

$$n_0(x) = \frac{I_0 L}{2AqD} \frac{\cosh(x/L)}{\sinh(W/2L)}$$

and

$$n_k(x) = \frac{I_k L_k}{2AqD} \frac{\cosh(x/L_k)}{\sinh(W/2L_k)}.$$

If $|\mathrm{RE}[n_k(x)/n_0(x)]|$ is less than unity, (1) may be expanded in a Taylor series as

$$v_i(t) = \frac{i(t)}{Aq\mu} \int_0^{W/2} \frac{dx}{n_0(x)} \cdot \sum_{l=0}^{\infty} (-1)^l \left\{ \sum_{k=1}^{K} \mathrm{Re} \left[ \frac{n_k(x)}{n_0(x)} e^{j\omega_k t} \right] \right\}^l. \quad (2)$$

Further approximation of (1) may be made using the following assumptions: 1) the lifetime of the carriers in the i-region is sufficiently large so that negligible recombina-

tion occurs, providing a nearly constant dc carrier density $[n_0(x) = n_0]$; 2) the frequency or frequencies of operation are sufficiently high so that $\omega\tau > 1$; and 3) all diode currents are in phase (which gives a "worst case" result in the distortion analysis [11]). Under these assumptions, the term in brackets in (2) may be written as

$$\frac{n_k(x)}{n_0(x)} e^{j\omega_k t} \cong \frac{I_k}{I_0}\frac{W}{L}\frac{1}{\sqrt{2\omega_k\tau}} \cdot \exp\left[\left(\frac{2x-W}{2L}\sqrt{\frac{\omega_k\tau}{2}}\right) + j\omega_k t\right]. \quad (3)$$

By writing the diode current as $I_i(t) = v_i(t)/R_s$ and taking the real part of (3), the total diode current can be written as

$$I_l(t) = \frac{2i(t)}{W}\sum_{l=0}^{\infty}(-1)^l \int_0^{W/2}\left\{\sum_{k=1}^{K}\alpha_k \cos\omega_k t\right\}^l dx \quad (4)$$

where

$$\alpha_k = \frac{I_k}{I_0}\frac{W}{L}\frac{1}{\sqrt{2\omega_k\tau}} \exp\left[(2x-W)\sqrt{\frac{\omega_k\tau}{2}} \Big/ 2L\right]$$

and $l$ is the order of distortion.

The restrictions on the Taylor series expansion can be written as

$$|\mathrm{RE}[n_k(x)/n_0]| = \frac{I_k}{I_0}\frac{W}{2L}(\omega_k\tau)^{-1/2} < 1. \quad (5)$$

The applicability range of the Taylor series expansion can be discussed through the use of an example. For a p-i-n diode with $\tau = 5$ μs and $W/2L = 1$ ($W = 90$ μm), the expansion is valid for RF signals up to about 20 times the forward bias current level at 10 MHz; thus, for 100 mA of forward bias, the model applies to RF drives of up to 2.0 A. For a device with $\tau = 0.5$ μs and $W/2L = 1$ ($W = 28$ μm), the model applies to RF drive currents up to 5.6 A at 1 GHz for 100 mA of forward bias.

The integrand in (4) contains the effects of the RF conductivity modulation by the applied ac signal and results in the generation of distortion components by the device. To find the distortion at any specific frequency, the integrand can be written as [11]

$$\left\{\sum_{k=1}^{K}\alpha_k \cos\omega_k t\right\}^l = \frac{2l!}{m!n!\cdots}\left[\left(\frac{\alpha_1}{2}\right)^m\left(\frac{\alpha_2}{2}\right)^n\cdots\right] \cdot \cos[(m\omega_1 \pm n\omega_2 \pm \cdots)t] \quad (6)$$

where $l = m + n + \cdots$. The final form for the nonlinear distortion currents produced by a p-i-n diode can then be written as ($l = 0$ being the fundamental)

$$I_l(t) = \sum_{l=1}^{\infty}\sum_{k=1}^{k}\beta_k \cos[(\omega_k \pm m\omega_1 \pm n\omega_2 \pm \cdots)t] \quad (7)$$

where

$$\beta_k = (-1)^l \frac{I_k}{W}\frac{2l!}{m!n!\cdots}2^{-l}\int_0^{W/2}(\alpha_1^m\alpha_2^n\cdots)\,dx.$$

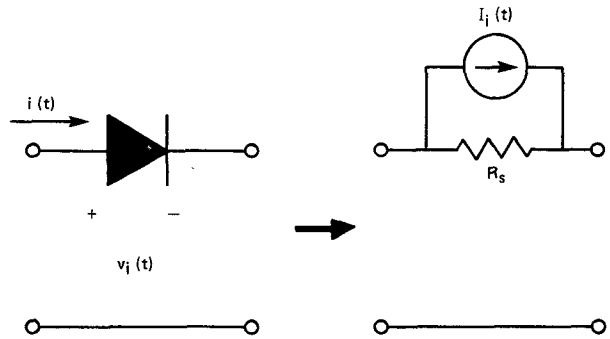


Fig. 3. The equivalent p-i-n diode circuit showing the dependent distortion current source $I_i(t)$.

The equivalent nonlinear circuit for the p-i-n diode is shown in Fig. 3. From (7), the distortion current at any frequency can be calculated for given input RF drive conditions and specified device parameters. Only values of $k = m, n \cdots$, related to the distortion frequency component desired, need be specified when solving for $\beta_k$ and $I_l(t)$ in (7).

### B. Model Interpretation

The form for the nonlinear diode current given in (7) is applicable to any circuit containing one or more devices. A discussion of the distortion in several control circuits using (7) in the presence of a single or two-tone RF drive signal follows. The discussion will be limited to second- and third-order distortion components, but may be extended to any higher order.

*1) Single-Device Circuits:* For frequencies $\omega_1$ and $\omega_2$, the second ($l = 1$) and third ($l = 2$) order harmonic and intermodulation load currents, respectively, can be found by solving (7), yielding the following expressions ($i, j = 1, 2$):

$$I_{H2} = -\frac{I_i^2}{I_0\omega_i\tau}\left(\frac{R_s}{R_s + 2Z_0}\right)$$

$$I_{H3} = \frac{\sqrt{2}}{8}\frac{W}{L}\frac{I_i^3}{I_0^2(\omega_i\tau)^{1.5}}\left(\frac{R_s}{R_s + 2Z_0}\right)$$

$$I_{\mathrm{IM2}} = -\frac{I_iI_j}{I_0\tau}\left(\frac{1}{\omega_i} + \frac{1}{\omega_j}\right)\left(\frac{R_s}{R_s + 2Z_0}\right)$$

$$I_{\mathrm{IM3}} = \frac{W}{\sqrt{2}L}\frac{I_i^2I_j}{I_0^2(\omega_i\tau)^{1.5}}\left[\frac{1}{4} + \frac{1}{\sqrt{\frac{\omega_j}{\omega_i} + \frac{\omega_j}{\omega_i}}}\right]\left(\frac{R_s}{R_s + 2Z_0}\right). \quad (8)$$

These expressions show that for closely spaced drive frequencies, the harmonic and intermodulation currents are related: $I_{\mathrm{IM2}} = 2I_{H2}$ and $I_{\mathrm{IM3}} = 3I_{H3}$. Higher order current components at any frequency can be found by solving (7) for the appropriate value(s) of $m, n, \cdots$.

The single figure of merit commonly used as a measure of distortion is called the intercept point [12]. The inter-

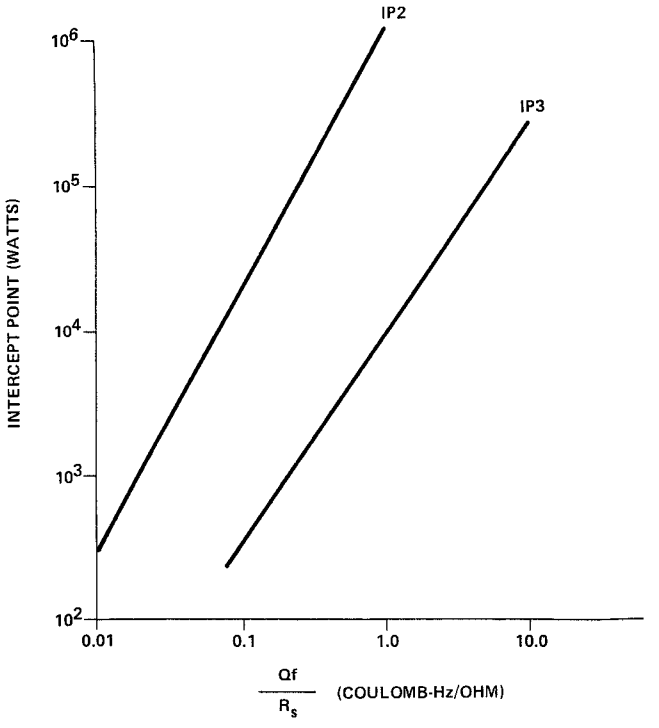


Fig. 4. Second- and third-order distortion intercept point versus the product $Qf/R_s$.

cept point is an extrapolation of the distortion power to the power level of the drive signals, assuming no compression of the drive signals. It is a fictitious power level, but provides a useful number from which distortion at any drive power may be computed. For the single-diode circuit (Fig. 2), the second (IP2) and third (IP3) order intercept points are found to be (assuming $I_1 = I_2 = I_{rf}$):

$$\text{IP2} = \frac{Z_0}{2}\left(\frac{R_s+2Z_0}{R_s}\right)^2 Q^2\left(\frac{1}{\omega_1}+\frac{1}{\omega_2}\right)^{-2}$$

$$\text{IP3} = \frac{Z_0}{2}\sqrt{V_T}\,\frac{2Z_0+R_s}{R_S^{3/2}}(\omega_1 Q)^{1.5} \cdot \left[\frac{1}{4}+\frac{1}{\frac{\omega_2}{\omega_1}+\sqrt{\frac{\omega_2}{\omega_1}}}\right]^{-1}. \quad (9)$$

*a) Switches:* For switch circuits where $R_s \ll Z_0$ and the frequencies are closely spaced ($f_1 \cong f_2 = f$), the second- and third-order intercept points may be written as

$$\text{IP2} = \frac{Z_0^3}{2}\left(\frac{2\pi fQ}{R_s}\right)^2 \quad \text{IP3} = 0.22Z_0^2\left(\frac{2\pi fQ}{R_s}\right)^{1.5}. \quad (10)$$

IP3 differs by a factor of 2 from the authors' earlier work, which used a different mathematical approach in analyzing p-i-n diode switch distortion [6]. In (10), the important factor controlling switch distortion at a specific frequency is the ratio $Q/R_s$ (Fig. 4). Since $Q = I_0\tau$ and $R_s = W^2/2\mu Q$ [10], then $Q/R_s$ is proportional to $(\tau/W)^2$.

In single-diode switch circuits, the distortion properties are improved if p-i-n diodes are selected or operated that

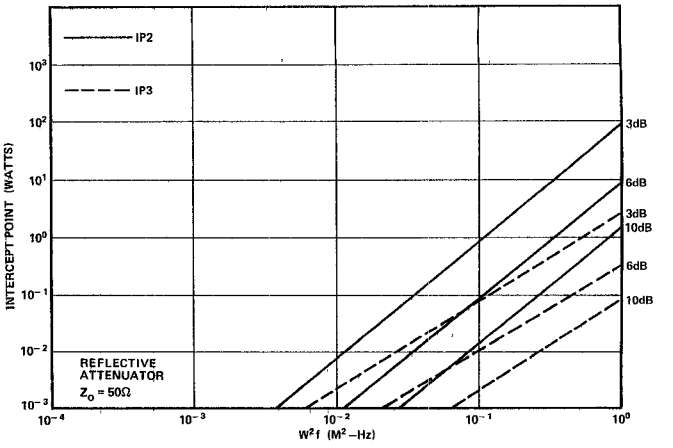


Fig. 5. Intercept point (watts) versus the p-i-n diode parameter $W^2f$.

maximize either the ratio $Q/R_s$ or $\tau/W$. Equation (10) shows that, at a fixed frequency, increasing the quantity $Q/R_s$ by a factor of 2 produces a fourfold increase (6 dB) in the second-order intercept point and a factor of 2.8 increase (4.5 dB) in the third-order intercept point. Distortion in single p-i-n diode switch circuits has been discussed and analyzed by Hiller and Caverly [6].

*b) Attenuators:* The identical circuit topology shown in Fig. 2 can be used as a reflective attenuator. In this case, the forward resistance ($R_s$) is controlled by varying the forward dc bias ($I_0$). If the attenuation level is defined as $A = [2Z_0/(R_s+2Z_0)]^2$, then the term $R_s/[R_s+2Z_0]$ in (8) may be replaced by $[1-\sqrt{A}]$, and the second- and third-order intercept points for this reflective attenuator can then be written as

$$\text{IP2} = \frac{1}{2}\left(\frac{W^2}{2\mu}\right)^2 \frac{A}{4Z_0(1-\sqrt{A})^4}\left(\frac{1}{\omega_1}+\frac{1}{\omega_2}\right)^{-2} \quad (11)$$

$$\text{IP3} = \frac{\sqrt{V_T}}{8}\left(\omega_1\frac{W^2}{2\mu}\right)^{1.5} \frac{A}{Z_0(1-\sqrt{A})^3} \cdot \left[\frac{1}{4}+\frac{1}{\frac{\omega_2}{\omega_1}+\sqrt{\frac{\omega_2}{\omega_1}}}\right]^{-1}.$$

Since $R_s$ is fixed for a given level of attenuation, solving for $Q/R_s$ (from $R_s = W^2/2\mu Q$ and $Q = I_0\tau$) shows the dependence of distortion only on $W$. Thus, in single-diode attenuators, the significant factor controlling distortion at a given attenuation level is the i-region width $W$. This clearly indicates that carrier lifetime ($\tau$) has no effect on attenuator distortion. The impact of $\tau$ on attenuator performance is, however, related to the current–resistance relationship. For example, devices of the same $W$ that differ in lifetime by a factor of 2 require one half the amount of forward bias current for the same resistance. Since the resultant $Q$ is the same in both cases, the distortion for both devices will be the same. Fig. 5 shows a plot of distortion intercept point versus $fW^2$ (calculated using (11)) for 3-, 6-, and 10-dB attenuation levels and at

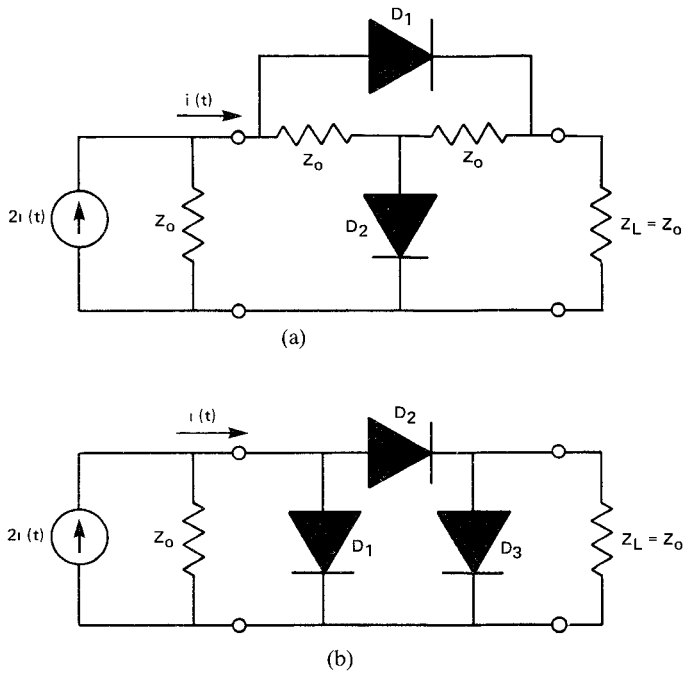


Fig. 6. Constant-impedance attenuator circuits: (a) bridged tee, and (b) PI.

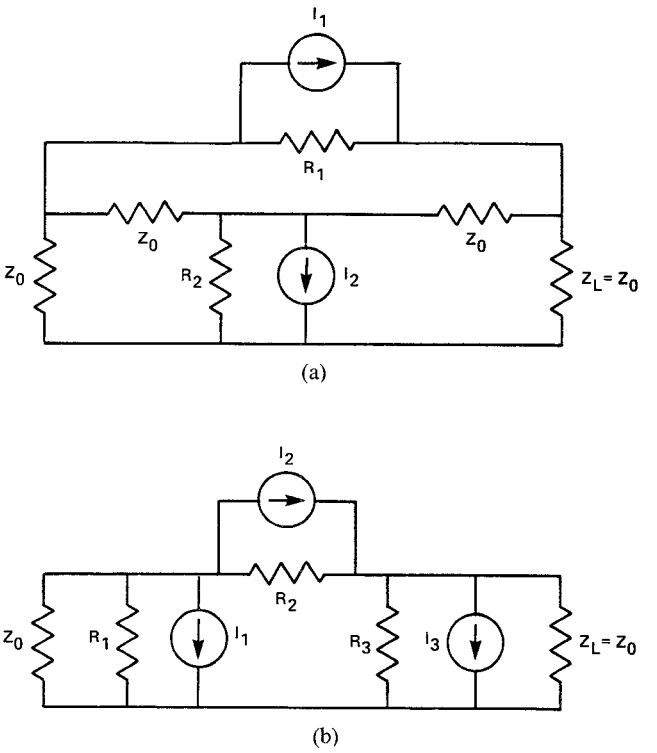


Fig. 7. Equivalent distortion circuits for the constant-impedance attenuator circuits shown in Fig. 6: (a) bridged tee and (b) PI.

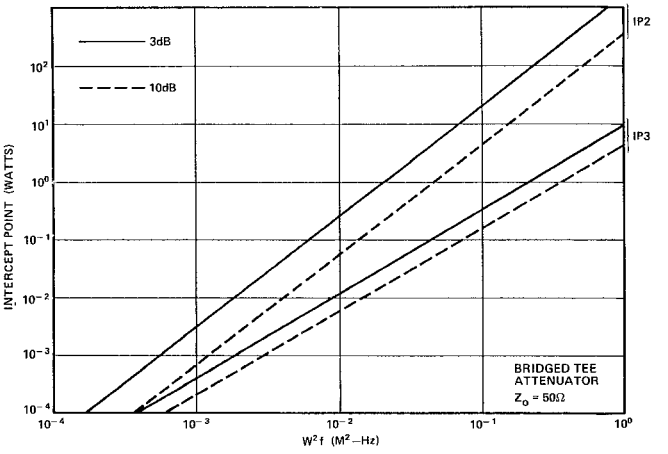


Fig. 8. Intercept point versus the p-i-n diode parameter $W^2f$ for 3- and 10-dB attenuation in the bridged tee attenuator.

nearly identical excitation frequencies, illustrating that the distortion intercept point increases with increasing i-region width.

The results presented in (10) and (11) show different figures of merit for p-i-n diodes used in switch and attenuator applications. They are both based on maximizing $Q/R_s$. In switch circuits, the ratio $\tau/W$ (high i-region lifetime and/or narrow i-region thickness) should be maximized for optimum distortion performance. For attenuator circuits, on the other hand, long i-region diodes result in improved distortion performance.

*2) Multiple p-i-n Diode Circuits:* The expression for the distortion currents given in (8) can be used in analyzing distortion in some familiar constant-impedance attenuator circuits (Fig. 6(a) and (b)) as well. The equivalent distortion circuits for these attenuators are shown in Fig. 7(a) and (b), and the output distortion voltages for the two circuits are presented in the Appendix. The resistance shown in each of these equivalent attenuator circuits is a function of the level of dc forward current applied to each p-i-n diode. In addition, since these are constant-impedance attenuator circuits, the value of the p-i-n diode resistance in each branch of the attenuator defines the attenuation level. Equations for resistance versus attenuation in these attenuator circuits have been presented by Hiller [13].

For a 50-Ω system, IP2 and IP3 for the "bridged-tee" attenuator at attenuation levels of 3 dB and 10 dB have been calculated and are shown in Fig. 8 versus the quantity $fW^2$. Fig. 9 presents information for the "PI" attenuator. These data have been calculated assuming nearly identical input excitation frequencies ($f_1 \cong f_2 = f$) and identical i-region widths. These calculations indicate that diodes with longer i-region widths generate lower levels of distortion under the same drive conditions independent of carrier lifetime. Also, doubling of the i-region width creates a fourfold decrease (6 dB) in the level of distortion power generated.

In the constant-impedance attenuators described, the distortion products have been observed to have a distinct minimum at specific levels of attenuation [2], [8], [9]. Using the previous analyses with matched diodes of 300-$\mu$m i-region lengths, input operating frequencies of 10 and 13 MHz, and an ac drive of 20 mA, distortion versus attenuation curves can be calculated (Fig. 10) that show both second- and third-order distortion signal cancellation occurring at 6-dB attenuation in the bridged-tee attenuator. Using identical diodes and operating conditions, the

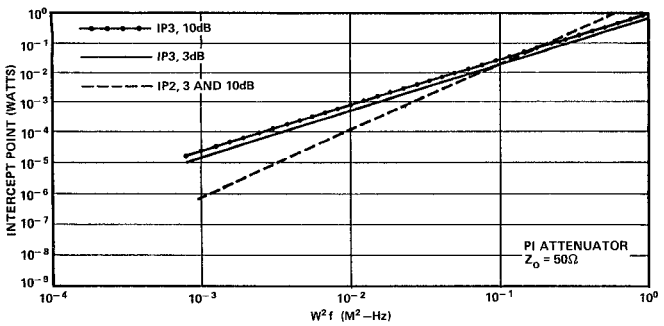


Fig. 9. Intercept point versus the p-i-n diode parameter $W^2f$ for 3- and 10-dB attenuation in the PI attenuator.

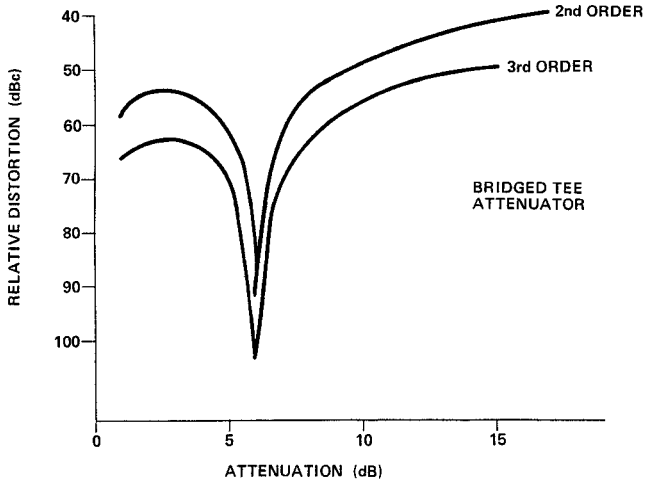


Fig. 10. Second- and third-order distortion (in dBc) versus attenuation level for the bridged tee attenuator.

third-order distortion signal cancellation occurs at 18 dB in the PI attenuator (Fig. 11). No second-order distortion signal cancellation occurs with matched diodes in the PI configuration according to this model.

The attenuation level where distortion signal cancellation occurs can be shifted to different levels of attenuation using p-i-n diodes of unequal i-region widths. Fig. 12 shows the attenuation level where distortion signal cancellation occurs versus diode i-region mismatch for the bridged-tee attenuator. The equal i-region width condition ($W_1/W_2 = 1$) shows cancellation at 6 dB. This phenomenon may be exploited by cascading attenuators, each with different cancellation points within a desired attenuation range.

## III. Experimental Results

Second- and third-order distortion measurements in switch circuits were performed centered at three frequencies, namely 7.5, 15, and 33 MHz, with the measured data in terms of distortion intercept point. The distortion intercept points derived earlier in (10) are presented in terms of dBm:

$$\text{IP2} = 34 + 20\log(Q_{\text{nC}} f_{\text{MHz}}/R_s)\,\text{dBm}$$
$$\text{IP3} = 24 + 15\log(Q_{\text{nC}} f_{\text{MHz}}/R_s)\,\text{dBm} \qquad (12)$$

where $Q_{\text{nC}}$ is the stored charge in nanocoulombs and $f_{\text{MHz}}$ is the operating frequency in megahertz. These experimen-

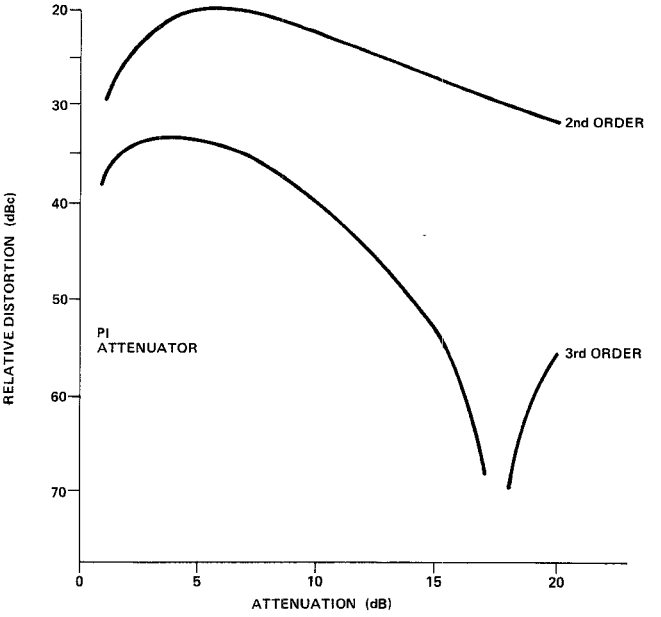


Fig. 11. Second- and third-order distortion (in dBc) versus attenuation level for the PI attenuator.

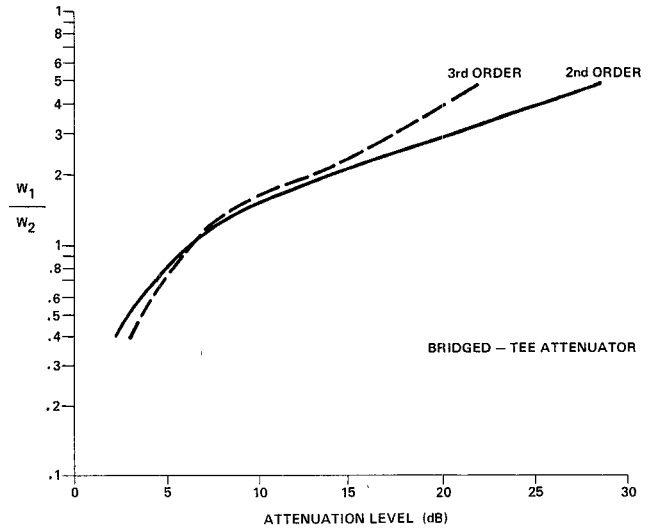


Fig. 12. Distortion signal cancellation point (in terms of attenuation level) versus i-region width ratio $W_1/W_2$.

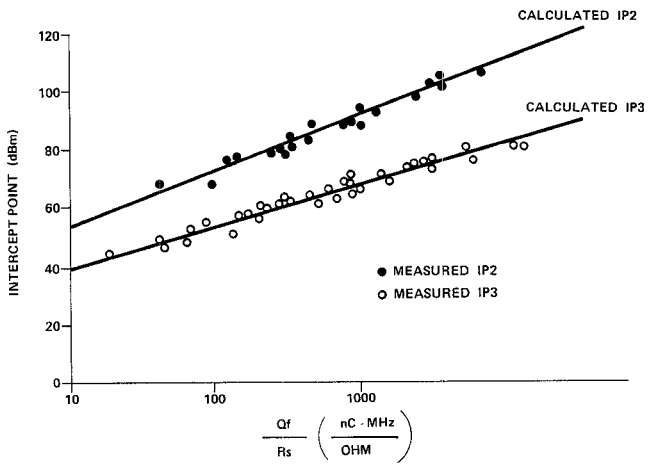


Fig. 13. Intercept point measurements and calculations from the p-i-n diode characteristics.

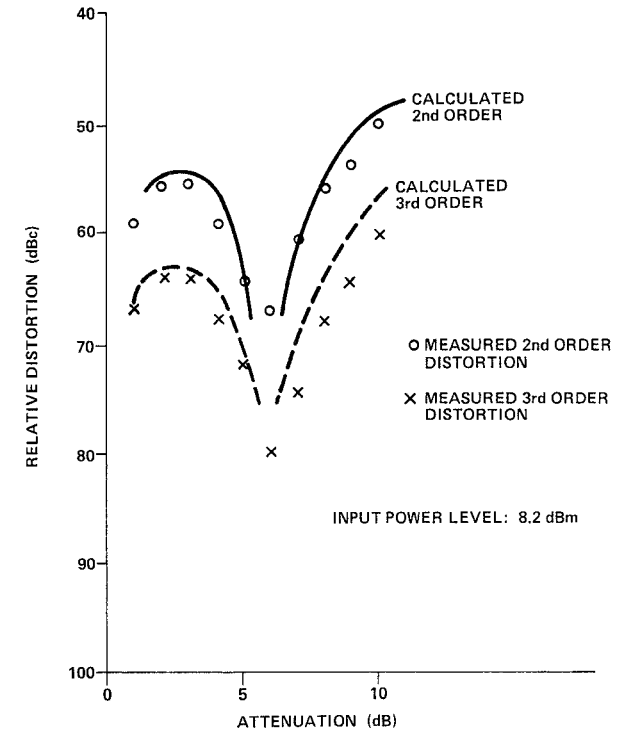


(a)

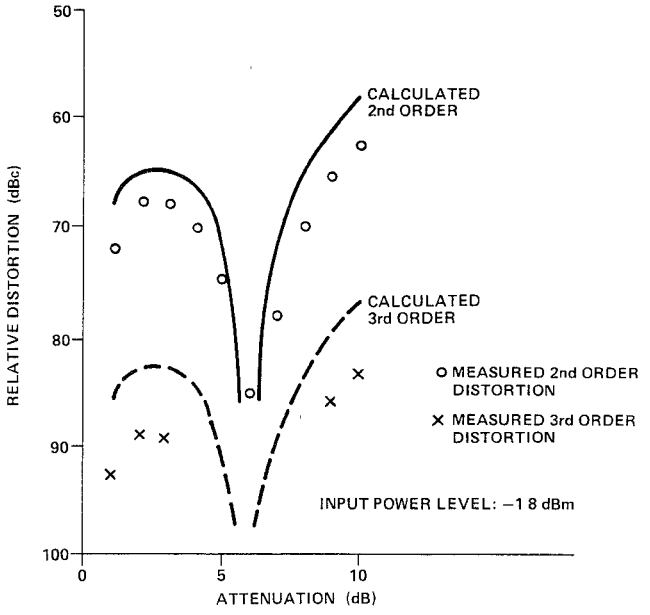


(b)

Fig. 14. Comparison of measured and calculated distortion levels for the bridged tee attenuator circuit: (a) 8.2 dBm and (b) −1 8 dBm.

tal data are plotted in Fig. 13 versus the quantity $Q_{nC} f_{MHz}/R_s$, with (12) plotted for comparison. Fig. 13 shows good agreement between the theoretical model for second- and third-order distortion intercept point and the experimental data. Inspection of (12) also reveals that a relationship between IP2 and IP3 exists and that IP3 can be written in terms of IP2 as follows:

$$\text{IP3} = 0.75\ \text{IP2} - 1.5\ \text{dBm}. \tag{13}$$

The distortion performance of a bridged-tee attenuator has been measured in the 10-MHz range with a 75-Ω system, commonly used in CATV applications. A comparison of the measured data and the theoretical model for second- and third-order distortion is presented in Fig. 14 for two values of ac drive, 8.2 dBm (Fig. 14(a)) and −1.8 dBm (Fig. 14(b)). Both diodes are matched and have 300-$\mu$m i-region widths. The effects of distortion signal cancellation at 6 dB are clearly seen as predicted by the model.

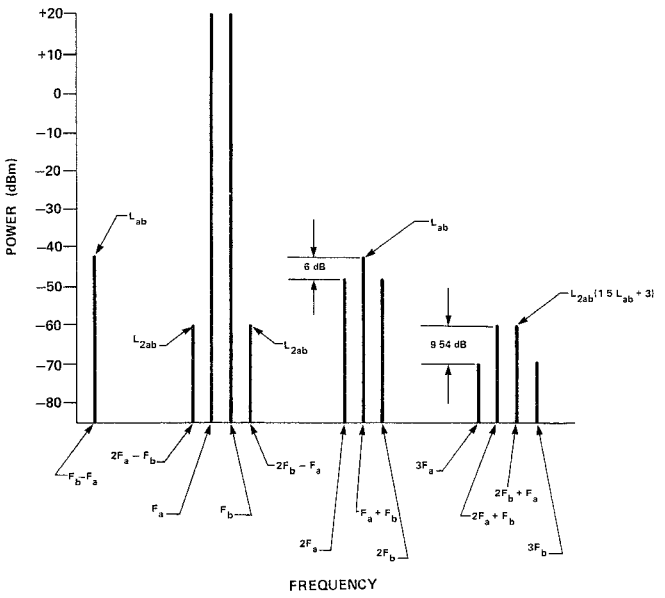


Fig. 15. Frequency spectrum of "behaving" distortion showing the fundamental signals and no distortion products higher than third order.

## IV. Spectrum

Since second- and third-order intercept points are related to each other as indicated in (13), the absolute power levels of third-order distortion may be computed from second-order distortion power levels. These relations are as follows for the second- and third-order harmonic power levels ($L_{2a}$ and $L_{3a}$) and the second- and third-order intermodulation power levels ($L_{ab}$ and $L_{2ab}$):

$$L_{2ab} = 1.5\ L_{ab} + 3\ \text{dBm}$$
$$L_{3a} = 1.5\ L_{2a} + 2.4\ \text{dBm}. \tag{14}$$

Fig. 15 shows the frequency spectrum of a p-i-n diode switch with a third-order intercept point of +60 dBm driven by two closely spaced +20-dBm signals. The distortion signals that are most detrimental to system performance are the third-order components adjacent to the carriers. These unwanted signals are not readily filterable. The expected intermodulation distortion levels for the same switch as a function of input power are shown in Fig. 16.

Equation (13), the relation between second- and third-order distortion, was experimentally verified by computing the third-order intercept point from a measurement of second-order distortion and comparing it to the derived third-order intercept point taken from third-order distortion measurements. This experimental verification is shown in Fig. 17. This good agreement between theoretical and experimental data allows the designer to predict third-order

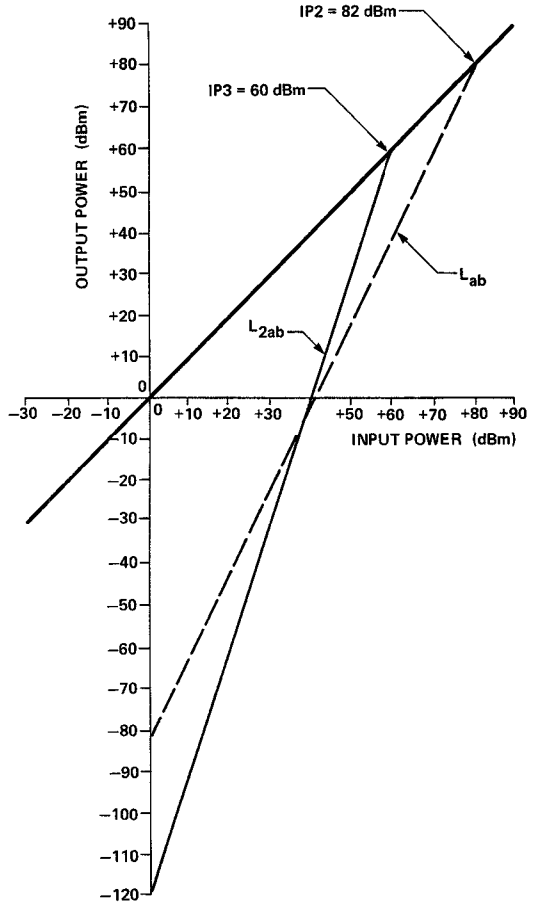


Fig. 16. The intercept point provides a convenient figure of merit from which distortion at any power level may be calculated.

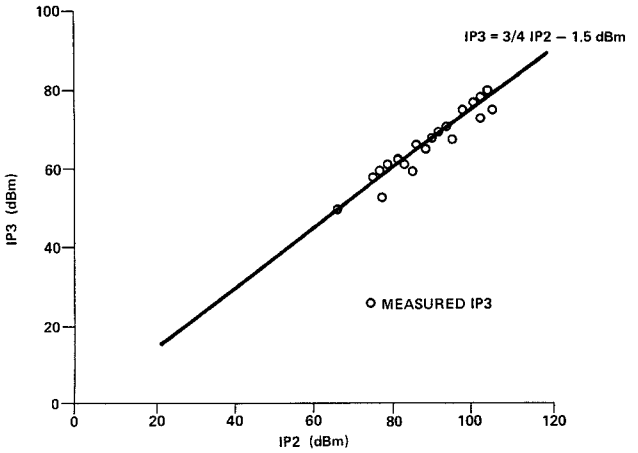


Fig. 17. Third-order intercept point measurements and calculation from second-order distortion measurements.

distortion from a direct measurement of second-order harmonic distortion without knowing the $Q$ and $R_s$ characteristics of the p-i-n diodes. This is useful since second-order distortion, because of its power level, is easier to measure than third-order distortion.

## V. Measurement Techniques

The measurement of distortion requires that the sources and spectrum analyzer be substantially free of internally generated distortion signals and that the device under test

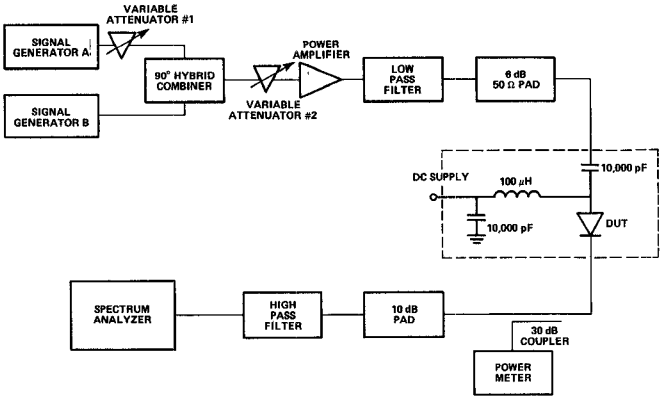


Fig. 18. Block diagram of the distortion test set.

see a constant impedance at all harmonic and intermodulation frequencies. The test set used to obtain the experimental data presented in this paper is shown in Fig. 18 and incorporates these principles.

The distortion measurements were all performed at power levels consistent with the device under test operating in its "behaving" distortion mode. This implies that the distortion products follow the second- and third-order exponential law. This was verified as follows.

1) The second-order IM products are 6.0 dB higher than second harmonics.
2) The third-order IM products are 9.45 dB higher than third harmonics.
3) Increasing the input power by 1.0 dB increases the level of second-order distortion by 2.0 dB and that of third-order distortion by 3.0 dB.
4) If one of the signals were removed, the harmonic levels of the remaining signals would not change.

## VI. C-Band Phase Shifter Application Example

Consider a 5-GHz switched line phase shifter designed to handle 1 kW of pulse power in a 50-Ω environment. The p-i-n diodes selected have a carrier lifetime of 0.1 μs and are rated for a resistance of 1 Ω maximum at the operating forward current of 100 mA. The circuit consists of cascaded switched line sections, each containing a SPDT switch at the input and output. Let us determine the relative second and third harmonic and intermodulation signals generated by each switched line section inserted by forward biasing the p-i-n diode on each side of the desired line length.

The stored charge on each forward-biased diode is computed from $Q = I_0\tau$ to 10 nC, and the second- and third-order intercept points per diode may be computed from (12) as 128 dBm and 94.5 dBm, respectively. At the 1-kW power level, the second- and third-order intermodulation signals compute to 68 dB and 69 dB below the carrier [6]. The second and third harmonics would be 74 dB and 78.5 dB below the carrier.

These numbers represent the distortion generated by the individual diodes at each end of the switched line element. Thus, the net second and third harmonic and intermodulation signals will be 3 dB higher than these numbers since each p-i-n diode acts as an individual distortion generator.

In addition, any additional line lengths added by pairs of forward-biased p-i-n diodes will further degrade the distortion by 6 dB. These predictions are based on having all harmonic frequencies perfectly matched.

## VII. Conclusions

The objective of this work was to give better understanding of the distortion mechanism in p-i-n diodes. The fundamental analytical conclusion reached is that the magnitude of the distortion signals generated is directly related to frequency ($f$) and the stored-charge-to-resistance ratio ($Q/R_s$) at the p-i-n diode operating point. The experimental data confirmed the analytic expressions.

In a p-i-n diode switch, where the p-i-n diode operates at a fixed forward bias current, the $Q/R_s$ ratio is maximized by maximizing the $\tau/W$ ratio in the diode. This will minimize the generated distortion. In a p-i-n diode attenuator, where the p-i-n diode is operated at a fixed resistance, it was shown that the $Q/R_s$ ratio is maximized by maximizing the i-region width ($W$) and that carrier lifetime ($\tau$) has no impact on distortion in an attenuator circuit. In all cases, distortion decreases with increasing frequency.

Analytic expressions were derived that will allow circuit designers to predict distortion levels. These expressions will also enable the device designer to model the p-i-n diode design for specific distortion requirements.

This paper demonstrates that the carrier lifetime of the p-i-n diode does not singularly determine distortion in a p-i-n diode circuit. It should be also understood that the material is limited to a forward-biased p-i-n diode operating under low or moderate power levels. This is typical of circuits used in receivers and synthesizers.

It is the authors' hope and expectation that additional analytic and experimental efforts will be made to establish the distortion mechanisms for the zero- or reverse-biased p-i-n diode and to provide relationships describing these distortion phenomena. Also, p-i-n diodes are being increasingly employed in transmitters, filters, and antenna coupler applications where power levels beyond 1 kW are being controlled at frequencies approaching 1 MHZ. A firmer understanding of distortion principles unde these conditions would be an important contribution to this technology.

## Appendix

### A. Bridged Tee Attenuator

Analysis of the equivalent distortion circuit shown in Fig. 7(a) for the T attenuator shows that the distortion voltage developed the load across $Z_1$ ($Z_1 = Z_g = Z_0$) can be shown to be

$$V_{ld} = \frac{Z_0}{2} \frac{R_2 I_2 (R_1 + Z_0) - R_1 I_1 (Z_0 + R_2)}{(R_1 + Z_0)(R_2 + Z_0)} \quad \text{(A1)}$$

where $I_1$ and $I_2$ are the distortion current generators described by (7) and are functions of the fundamental ac drive current flowing through diodes $D_1$ and $D_2$ (Fig. 6(a)). The ac drive current through each diode is a function of the resistance required for a matched attenuator.

### B. PI Attenuator

Analysis of the equivalent distortion circuit for the PI attenuator shown in Fig. 7(b) shows that the distortion developed across the load resistance can be written as ($Z_1 = Z_g = Z_0$ and $R_1 = R_3 = R_p$):

$$V_{ld} = \frac{Z_0}{Z_0 + R_p} \frac{R_p I_3 \left[ (Z_0 + R_p)(R_p + R_2) - R_p^2 \right] + R_p^2 Z_0 I_1 - R_2 R_p (Z_0 + R_p) I_3}{(Z_0 + R_p)(2R_p + R_2) - 2R_p^2}. \quad \text{(A2)}$$

The distortion currents $I_1$, $I_2$, and $I_3$ are functions of the fundamental ac drive current flowing through diodes $D_1$, $D_2$, and $D_3$ (Fig. 6(b)).

## Acknowledgment

Some of the measurements reported in this article were performed at Unitrode Corp., Watertown, MA. The authors would also like to thank the reviewers for their valuable comments regarding the manuscript; their suggestions enhanced the readability and understanding of the paper.

## References

[1] D. Leenov, "The silicon PIN diode as a microwave radar protector at megawatt levels," *IEEE Trans. Electron Devices*, vol. ED-12, p. 53, Feb. 1965.

[2] J Lepoff, "A new PIN diode for UHF–VHF applications," *IEEE Trans Broadcast Telev. Receivers*, vol. BTR-17, pp. 10–15, Feb. 1971.

[3] M. Caulton, A. Rosen, P. Stabile, and A. Gombar, "p-i-n diodes for low frequency–high power switching application," *IEEE Trans. Microwave Theory Tech.*, vol. MTT-30, p. 875, June 1982.

[4] R. Sicotte and R. Assaly, "Intermodulation products generated by a PIN switch," *Proc. IEEE*, vol. 56, p. 74, Jan. 1968.

[5] D. Mott and D. McQuiddy, "The harmonics produced by a PIN diode in a microwave switching applications," *IEEE Trans. Microwave Theory Tech.*, vol. MTT-15, p. 180, 1967.

[6] G Hiller and R. Caverly, "Predict PIN-diode switch distortion," *Microwaves and RF*, vol. 25, no. 1, p. 111, Jan. 1986.

[7] C. Albrecht and F. Jansen, "Numerical analysis of nonlinear small-signal distortion in p-n structures," *IEEE Trans. Electron Devices*, vol. ED-24, p. 91, Feb. 1977.

[8] W. Reiss, "Volterra series representation of a forward biased p-i-n diode," *IEEE Trans. Electron Devices*, vol. ED-28, p. 1495, Dec. 1981.

[9] W. Reiss, "Nonlinear distortion analysis of p-i-n diode attenuators using Volterra series representation," *IEEE Trans. Circuits Syst.*, vol. CAS-31, p. 535, June 1984.

[10] J. White, *Microwave Semiconductor Engineering*. New York: Van Nostrand Reinhold, 1981.

[11] W Gretsch, "The spectrum of intermodulation generated in a semiconductor diode junction," *Proc. IEEE*, vol. 54, p. 1528, Nov. 1966.

[12] G. Heiter, "Characterization of nonlinearities in microwave devices and systems," *IEEE Trans. Microwave Theory Tech.*, vol. MTT-21, p. 797, Dec. 1973.
[13] G. Hiller, "Design with PIN diodes," *RF Design*, Mar./Apr. and May/June 1979.

✠

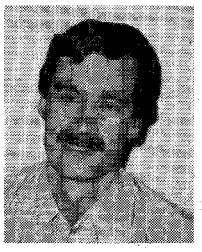

**Robert H. Caverly** (S'79–M'83) was born in Cincinnati, OH, in 1954. He received the M.S.E.E. and B.S.E.E. degrees from North Carolina State University, Raleigh, NC, in 1978 and 1976, respectively. He received the Ph.D. degree in Electrical Engineering from The Johns Hopkins University, Baltimore, MD, in 1983.

He has been employed at Southeastern Massachusetts University as an Assistant Professor since 1983. He has also been a consultant for M/A-COM during that time period. In 1985, he was appointed Director of the University's Computer Aided Engineering Laboratory, and he is currently involved with the Massachusetts Microelectronics Center. In addition to his interest in computer-aided engineering in microelectronics, he is also interested in the application of computer software to microwave engineering problems. Dr. Caverly's current efforts are involved with characterizing the p-i-n diode in the RF environment and in characterizing integrated gallium arsenide magnetic field sensors.

✠

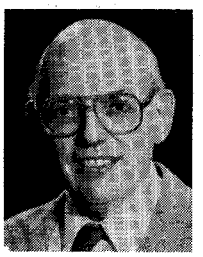

**Gerald Hiller** (S'56–M'58) was born in New York City, NY. He received the B.E.E. degree from the City College of New York in 1958 and the M.S.E.E. degree from the University of Pennsylvania in 1963.

From 1958 to 1962, he was employed by Philco Corporation, Philadelphia, PA, where he developed microwave circuits using semiconductor devices with special emphasis on mixer diodes and millimeter receivers. From 1962 to 1972, he was with the Micro State Electronics Operation of Raytheon Company, Murray Hill, NJ, where he was involved with control circuits, amplifiers, and multipliers and served as Semiconductor Applications Manager. From 1972 to 1984, he served as Director of Microwave Engineering at Unitrode Corporation, Watertown, MA, where he was active in the development of Unitrode's p-i-n diode product line. In this capacity, he wrote many technical papers pertaining to the use of p-i-n diodes at RF and UHF. In 1984, Mr. Hiller joined M/A-COM Semiconductor Products Inc., Burlington, MA, as Manager of Semiconductor Applications. His current efforts are involved with characterizing silicon and GaAs p-i-n diodes and their circuit applications.